Stable many-body localization under random continuous measurements in the no-click limit

Giuseppe De Tomasi[1] and Ivan M. Khaymovich[2,3]

[1]*Department of Physics, University of Illinois at Urbana-Champaign, Urbana, Illinois 61801-3080, USA*

[2]*Nordita, Stockholm University, and KTH Royal Institute of Technology, Hannes Alfvéns väg 12, SE-106 91 Stockholm, Sweden*

[3]*Institute for Physics of Microstructures, Russian Academy of Sciences, 603950 Nizhny Novgorod, GSP-105, Russia*

(Received 25 November 2023; revised 11 April 2024; accepted 1 May 2024; published 10 May 2024)

In this work, we investigate the localization properties of a paradigmatic model, coupled to a monitoring environment and possessing a many-body localized (MBL) phase. We focus on the postselected no-click limit with quench random rates, i.e., random gains and losses. In this limit, the system is modeled by adding an imaginary random potential, rendering non-Hermiticity in the system. Numerically, we provide evidence that the system is localized for any finite amount of disorder. To analytically understand our results, we extend the quantum random energy model (QREM) to the non-Hermitian scenario. The Hermitian QREM has been used previously as a benchmark model for MBL. The QREM exhibits a size-dependent MBL transition, where the critical value scales as $W_c \sim \sqrt{L}\ln L$ with system size and presenting many-body mobility edges. We reveal that the non-Hermitian QREM with random gain-loss offers a significantly stronger form of localization, evident in the nature of the many-body mobility edges and the value for the transition, which scales as $W_c \sim \ln^{1/2} L$ with the system size.

DOI: 10.1103/PhysRevB.109.174205

I. INTRODUCTION

Generic closed quantum many-body systems tend to thermalize under their own time evolution, erasing the microscopic details of their initial conditions [1–3]. In such systems, the final steady state is characterized by a small set of globally conserved quantities and the system obeys the law of statistical mechanics.

The investigation of nonequilibrium phenomena in quantum systems has unveiled new phases of matter. These phases usually lack counterparts in equilibrium states and could be crucial for enhancing the robustness of quantum computing. To enhance coherence, several mechanisms have been suggested to impede thermalization, thus preserving critical quantum correlations essential for quantum computing. A prime example of this is the phenomenon known as many-body localization (MBL) [4–7] which extends the Anderson localization to the many-body case. The strong quenched disorder prevents many-body systems from thermalizing, leading to localization. This ergodicity breaking manifests itself in the system's quantum dynamics [8–16]. The local memory of the initial state is preserved during time evolution, attributed to a "robust" form of an emergent integrability. Consequently, the system can be fully described by an extensive set of quasilocal integrals of motion [15–21]. Later, alternative mechanisms for (weak) ergodicity breaking were suggested, ranging from quantum many-body scars and Hilbert-space fragmentation [22–26] to the localization in lattice gauge theories [27–30].

Recently, there has been a growing interest in nonunitary quantum dynamics, both from theoretical and experimental perspectives. A notable instance is the recent exploration of monitored quantum systems [31–34]. In these systems, the unitary dynamics of typical quantum systems, which scramble and increase the entanglement of the state, are in competition with the continuous measurement of local observables, which locally projects the system into the low-entanglement states. This results in an intricate spreading of entanglement and correlations during the dynamics. Numerous studies have highlighted the existence of a distinct phase transition triggered by measurements [33–37], dubbed the measurement-induced entanglement transition. This transition is commonly characterized by the scaling of entanglement dynamics and distinguishes between a volume-law phase, where entanglement scales with the volume of the system, and an area-law phase, where it grows as the boundary of the partition.

Static non-Hermitian quantum systems can describe some of the nonunitary dynamics mentioned above. For example, the non-Hermitian description arises naturally in the so-called "no-click limit," where the system is continuously monitored [38–49]. Then one postselects the quantum trajectories corresponding to no-measurement events. Several many-body systems, ranging from the transverse-field Ising model to the long-range Kitaev chain, show the existence of the entanglement transition, both in the dynamics and in the steady state properties [39,41,50–53].

Generically, the study of non-Hermitian many-body systems has emerged as a new paradigm for describing open, dissipative, and monitored systems. The non-Hermitian systems uncover a rich phenomenology and the study of them is an active research front, describing unique effects, ranging from generalized topological phases and new forms of

quantum criticality [54] to entanglement transitions that are not possible in the Hermitian counterparts. For instance, one of the most celebrated effects is a so-called non-Hermitian skin effect [55–57], where eigenstates of a non-Hermitian system localize at the boundary of a lattice, arising due to nonreciprocal hopping across the system with open boundary conditions. This effect challenges the conventional wisdom of the bulk-boundary correspondence in topological systems. Furthermore, it has been shown that such a skin effect suppresses entanglement propagation and thermalization and even induces an entanglement phase transition [58].

In general, non-Hermiticity is responsible for an increase in decoherence and might break localization. Hatano and Nelson in their seminal work [59] show that even in one dimension, where the short-range Hermitian systems are localized for any finite amount of disorder, strong nonreciprocity in hopping breaks the Anderson localization, creating energy bands of delocalized states. The fate of the Hatano-Nelson model in the presence of interaction has been recently studied in several works [60–65], showing the existence of a stable MBL phase for both weak disorder and non-Hermiticity.

In this work, we focus on a paradigmatic model, hosting the MBL transition under random continuous monitoring in the so-called no-click limit. In this limit, the model maps to a non-Hermitian Hamiltonian having complex random fields, which can be seen as random gain and loss terms or coupling to local inhomogeneous baths of random strength. We inspect several probes to the extension and the entanglement properties of their eigenstates. We provide numerical evidence that the critical disorder amplitude scales down with the system size, implying that the system is localized for any finite amount of disorder in the thermodynamic limit. To grasp an analytical understanding of this robust localization, we inspect a non-Hermitian version of the MBL proxy, namely, the quantum random energy model (QREM). The Hermitian QREM is a "mean-field" model describing more realistic and local MBL systems. Generalizing the self-consistent theory of localization to the non-Hermitian QREM, we show that the non-Hermiticity results in parametrically stronger localization than in its Hermitian counterpart. This effect is mainly based on the increase of the effective dimensionality of the diagonal disorder, leading to a parametric increase in the level spacing and, thus, reducing the number of resonances responsible for the delocalization.

The rest of the work is organized as follows. In Sec. II we describe the non-Hermitian modification of a paradigmatic MBL model, followed by the numerical results in Sec. III. Section IV provides the analytical consideration of a non-Hermitian version, Sec. IV A, of a proxy QREM model for both finite, Sec. IV C, and zero, Sec. IV D, energy density. We conclude our consideration in Sec. V.

II. MODEL AND METHODS

We consider the random-field Heisenberg chain of size L,

$$H_0 = \sum_x^L S_x^+ S_{x+1}^- + \text{H.c.} + \Delta S_x^z S_{x+1}^z + W \sum_x^L \mu_x S_x^z, \quad (1)$$

subject to a random monitoring environment in the "no-click" limit. $-1 \leqslant \mu_x \leqslant 1$ is the random field and we use periodic boundary conditions $S_{L+1} = S_1$. We set the interaction Δ to be $\Delta = 1$ and W is the strength of the random field. The model conserves the total magnetization $M = \sum_x S_x^z$, and we consider the largest sector with zero magnetization ($M = 0$).

Without monitoring, the model is known to exhibit an MBL transition, separating an ergodic phase from a localized one, around $W_{\text{MBL}} \approx 4$–6 in the middle of its spectrum [66–74]. For $\Delta = 0$, the system is Anderson localized for any finite amount of disorder $W > 0$ [75,76].

We consider the limit of postselection, also called the forced measurement phase or no-click limit [38–45], in which the system is modeled by a non-Hermitian Hamiltonian,

$$H = H_0 + iW' \sum_x \gamma_x L_x^\dagger L_x, \quad (2)$$

where L_x are Kraus operators $L_x = 2S_x^z + 1$ from the Lindbladian formalism. We consider coupling amplitudes γ_x to be random $|\gamma_x| \leqslant 1$ [77], having in mind a system, coupled to the set of L local baths of random size and coupling. In the last sentence, we appeal to physical argumentation beyond the Lindblad formalism, where the bath size is assumed to be infinite from the outset. In experimentally feasible setups with several local baths, the coupling typically depends on the number of modes in the corresponding bath (see, e.g., [78]). W' represents the strength of the random dissipation term.

Through the Jordan-Wigner transformation, the above non-Hermitian Hamiltonian is equivalent to the fermionic hopping model with the local density-density interaction between nearest-neighbor sites, subject to random on-site disorder and random gain and loss terms. The monitored system in the noninteracting limit, $\Delta = 0$, is also localized under the effect of random gain and loss in both the short-range Anderson [79,80] and long-range [81,82] settings. In Ref. [60] a similar model with staggered but nonrandom gain and loss has been considered to confirm the existence and the stability of an MBL phase at strong disorder.

To understand the fate of the MBL transition under monitoring of the model in Eq. (2), we investigate the localization properties of the right eigenvector belonging to the middle of the spectrum of H [83],

$$H\,|E_n\rangle = E_n\,|E_n\rangle\,. \quad (3)$$

Similarly to the Hermitian case, the choice of the middle of the spectrum is related to the fact that there the density of states,

$$\rho\big(E_0 = E_0^R + iE_0^I\big) = \sum_n \delta\big(E_0^R - \text{Re}\,E_n\big)\delta\big(E_0^I - \text{Im}\,E_n\big), \quad (4)$$

is maximal, which implies the smallest mean level spacing and the most delocalized states in the disordered systems to be in that part of the spectrum. In our numerical considerations we have focused on the localization transition of those most delocalized states in the system, and therefore consider $|E_0|/L \to 0$.

With this aim, we consider the half-chain bipartite entanglement entropy,

$$S(L/2) = -\text{Tr}[\rho_{L/2} \ln \rho_{L/2}], \quad (5)$$

with the reduced density matrix $\rho_{L/2}$ of the state in a half chain. The ergodic behavior of S in Hermitian systems is known to be represented by the so-called Page value $S_{\text{Page}} = (L \ln 2 - 1)/2$ [84], with some finite deviations, claimed later [85–89]. Here and further, we omit the argument $(L/2)$, focusing only on the half-chain partitions. In general, we indicate the disorder and eigenstate average with an overbar on the considered quantity, i.e., $\overline{S}$. As a further probe, we consider fluctuations over a few eigenstates and disorder configurations $\overline{\delta S^2} \equiv \overline{S^2} - \overline{S}^2$.

From the Hermitian systems' point of view, in an extended phase, we expect $\overline{S}$ to scale linearly with system size L, while in the localized, $\overline{S}$ should have an area-law scaling, $\overline{S} \sim O(L^0)$. Instead, the fluctuations decay exponentially with system size in the ergodic phase and do not scale with L in the localized phase. These two behaviors are interpolated by diverging fluctuations, $\overline{\delta S^2} \sim L^2$, around the transition ($W \approx W_{\text{MBL}}$). It is widely known that due to the entanglement and the correlations to the bath(s), the open quantum system is in a mixed state, where the entanglement entropy contains the correlations of a chosen subsystem not only to the rest of the system itself, but also to the corresponding baths. In the non-Hermitian setup (no-click limit), the dephasing of the system due to the measurement backaction is formally absent in the framework, keeping the system in a pure state. We will focus on the localized part of the phase diagram, where S obeys an area law and estimates the area-law growth of the entanglement between subsystems themselves. In such a way we will get a good estimate of the critical disorder amplitude W_{MBL}.

In the Hermitian case, it has been observed that the finite-size estimate of the critical point W_{MBL} shifts to the larger values with increasing system sizes L. Several numerical works using finite-size techniques have shown that this shift is consistent with the existence of a genuine MBL transition at a finite value [67,73,90–93]. However, recently, other works have questioned these results [94–96], proposing that only a finite-size transition is possible, whose critical value is proportional to the system size $W_{\text{MBL}} \sim L$.

We also investigate the spread of eigenstates in the Hilbert space, quantified by the inverse participation ratio

$$IPR_2 = \sum_{\underline{\sigma}} |\langle \underline{\sigma} | E_n \rangle|^4, \tag{6}$$

where $\{|\underline{\sigma}\rangle\}$ is the full set of the σ^z basis states and $|E_n\rangle$ is the eigenstate of the above Hamiltonian with the eigenvalue E_n. From IPR_2, we extract its fractal dimension D_2,

$$IPR_2 \sim (\dim \mathcal{H})^{-D_2}, \tag{7}$$

where $\dim \mathcal{H} = \binom{L}{L/2}$ is the dimension of the Hilbert space in the zero-magnetization sector. For ergodic states, $D_2 \to 1$ in the thermodynamic limit, while generic nonergodic states will have fractal behavior, meaning $0 < D_2 < 1$. For the Hermitian case, it has been shown that $D_2 \approx 1$ in the thermal phase and $0 < D_2 < 1$ in the MBL phase [67,90,92,97]. It has also been argued that D_2 exhibits a jump at the transition. The fluctuations of D_2 over eigenstates and disorder configurations, $\delta D_2^2 = \overline{D_2^2} - \overline{D_2}^2$, provide a remarkable fingerprint of the transition. δD_2^2 should be exponentially suppressed with L in the ergodic phase [$\delta D_2^2 \sim O(e^{-\alpha L})$], only algebraically in the MBL phase [$\delta D_2^2 \sim O(L^{-1})$], and δD_2^2 stays finite [$\delta D_2^2 \sim O(1)$] at the critical point, due to the above jump in D_2 [97]. Further, we focus on the fluctuations of $\ln IPR_2$, $\delta \ln IPR_2^2 = \delta D_2^2 L^2$.

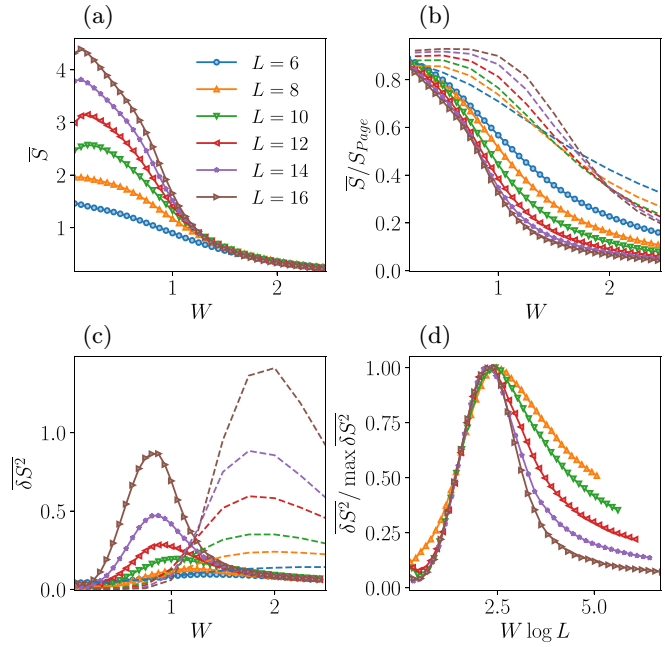

FIG. 1. MBL model: Entanglement entropy and its fluctuations in a non-Hermitian setting of Eq. (2). (a) $\overline{S}$ and (b) $\overline{S}/S_{\text{Page}}$ as functions of W for several system sizes L. (c) Bare entanglement fluctuations $\overline{\delta S^2}$ and (d) their value, normalized by the maximum value. In panel (d) the disorder strength has been renormalized by multiplying by $\ln L$. Dashed lines in panels (b), (c) show the corresponding measures for the equivalent Hermitian Hamiltonian, Eq. (8).

III. NUMERICAL RESULTS

We start our investigation with the examination of the entanglement entropy and its fluctuations as a function of disorder strength $W = W = W'$, focusing on the right eigenvectors from the middle of the spectrum of H in Eqs. (1) and (2).

Figures 1(a) and 1(b) depict the average half-partition entanglement entropy, Eq. (5), and the ratio $\overline{S}/S_{\text{Page}}$ (represented by solid lines), respectively. Here, the Page value S_{Page} will be used as a reference value, being the expected value for ergodic states at infinite temperature (middle of the spectrum). The rest of the figure, Figs. 1(c) and 1(d), showcases the fluctuations of S.

Notably, $\overline{S}/S_{\text{Page}}$ decreases as the system size increases, and the peak of its fluctuations also appears to systematically move to a smaller value of W; see Fig. 1 [98]. This behavior may suggest the presence of a finite-size crossover between a volume-law phase and an area-law phase. However, the volume-law phase seems to vanish in the thermodynamic limit.

To support these observations, it is valuable to compare them with the Hermitian case, which is believed to exhibit the

MBL transition at finite $W = W_{\mathrm{MBL}}$. For a fair comparison between the Hermitian and the non-Hermitian settings described in Eq. (2), we examine the Hamiltonian, where the complex disorder is replaced by the real one of the same amplitude,

$$H_h = H_0 + W' \sum_x \gamma_x L_x^\dagger L_x, \tag{8}$$

as depicted by dashed lines in Figs. 1(b) and 1(c). First, we observe that in the Hermitian case the finite-size crossover between the thermal and the ergodic phases happens at larger disorder, indicating that the non-Hermitian part tends to localize the system. This is particularly evident in Fig. 1(b), where the dashed lines present a crossing point in the proximity of the putative MBL transition. Indeed, $\overline{S}/S_{\mathrm{Page}} \to 1$ as the system size grows for the weak disorder, while $\overline{S}/S_{\mathrm{Page}} \to 0$ at larger disorder. However, for the non-Hermitian case, we have $\overline{S}/S_{\mathrm{Page}} \to 0$ with growing L for all available W. The enhancement of localization due to non-Hermiticity is also visible in the fluctuation of S; cf. dashed and solid lines in Fig. 1(c). First, the maximum of $\overline{\delta S^2}$ is higher in the Hermitian case; second, it happens at larger disorder; and finally, we observe the typical shifting of the maximum to the larger values of disorder only in the Hermitian case, but not in its non-Hermitian counterpart. We can conclude that this non-Hermiticity enhanced its localization properties.

Realizing that the system tends to the localization with increasing L, we analyze a finite-size scaling of $\overline{\delta S^2}$ as a function of W. As shown in Fig. 1(d), we have found a remarkably good collapse of the left wing of the $\overline{\delta S^2}$ maximum by rescaling the disorder strength, $W \to W \ln L$. This collapse provides evidence that the parameter space hosting an extended phase shrinks with systems size as $\sim 1/\ln L$. As the considered entanglement entropy S provides only an estimate of the entanglement between subsystems themselves, the above results provide the critical disorder W_{MBL}. As this estimate goes toward zero in the thermodynamic limit, we have to conclude that the critical disorder also does that.

To bolster our findings, we delve into the wave-function Hilbert-space spreading via the fractal dimension D_2, defined by Eq. (7), as depicted in Fig. 2. Indeed, in Figs. 2(a) and 2(c), we display the results for $\overline{D_2}$ and the fluctuations $\overline{\delta \ln IPR_2{}^2}$ of the IPR as functions of W for various values of L. Consistently with the above entanglement entropy data, the fractal dimension D_2 is significantly below its ergodic value, $D_2 = 1$, and the data show only a mild dependence on L, and mostly for relatively small values of W. The IPR fluctuations, $\overline{\delta \ln IPR_2{}^2}$ in Fig. 2(c), diverge with increasing L, approximately at the same W value as $\overline{\delta S^2}$ in Fig. 1. Analogously to $\overline{\delta S^2}$, the peak of $\overline{\delta \ln IPR_2{}^2}$ flows to lower W values, as L increases. Moreover, while $\overline{\delta \ln IPR_2{}^2} \sim L$ is evident in the presence of strong disorder, as expected in a localized phase, there is no observed exponential suppression at weak-disorder values. This further justifies the probable absence of an extended phase in the thermodynamic limit.

As we previously did by analyzing the entanglement entropy in Fig. 1, it is crucial to compare this result with the results of the Hermitian case in Eq. (8). The corresponding data are presented in Fig. 2(b), illustrating $\overline{\delta \ln IPR_2{}^2}$, while

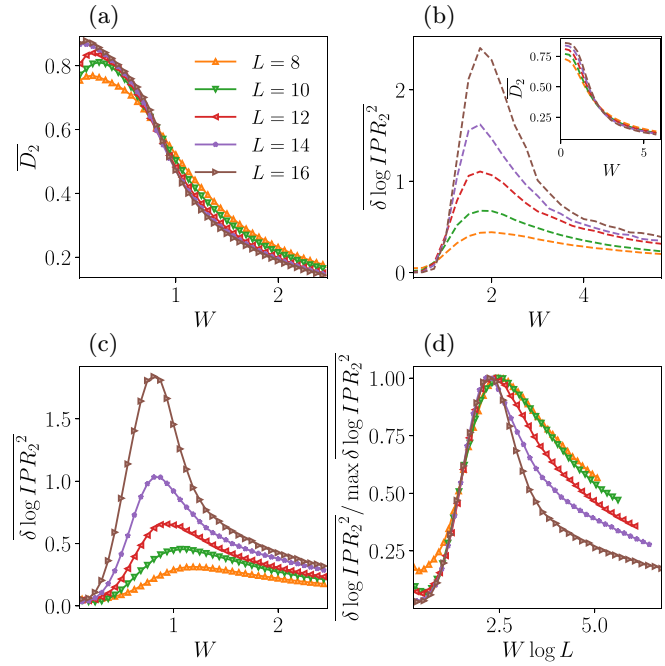

FIG. 2. MBL model: Fractal dimension D_2 and its fluctuations in a non-Hermitian setting of Eq. (2). (a) $\overline{D_2}$ as a function of W for several L, Eq. (7). (b) shows the fluctuations of $\ln IPR_2$ in the Hermitian case of Eq. (8); inset shows the corresponding $\overline{D_2}$ vs W. (c) Bare fluctuations $-\overline{\delta \ln IPR_2{}^2}$ of $-\ln IPR_2$ and (d) their value, normalized by the maximum value. In panel (d) the disorder has been renormalized as follows: $W \to W \ln L$.

the inset shows $\overline{D_2}$ vs W. Supporting the insights from the entanglement entropy, the IPR data underscore the propensity of non-Hermitian components to enhance the system's localization. Conclusively, a robust convergence for the fluctuations of the fractal dimension is evident in Fig. 2(d), attesting that the extended phase diminishes in the thermodynamic limit, scaling as $1/\ln L$.

Finally, Fig. 3 shows entanglement entropy and its fluctuations for eigenstates in the middle of the spectrum for different real and imaginary disorder strengths $W = 2W'$. Although the dissipation term has half strength of the random potential, $W = 2W'$, we do not see qualitative difference and all its eigenstates are area law in the limit $L \to \infty$.

In summary, through the examination of multiple complementary indicators, we present numerical proof that our monitored random-field Heisenberg model exhibits the localization in the thermodynamic limit, irrespectively of the disorder magnitude.

Entanglement dynamics

Here we provide further investigation considering dynamical probes. In particular, we consider the entanglement dynamics

$$|\psi(t)\rangle = \frac{e^{-itH}|\psi(0)\rangle}{\|e^{-itH}|\psi(0)\rangle\|}, \tag{9}$$

starting from a random pure state $|\psi(0)\rangle$. Here $\|\ldots\|$ is the norm of the corresponding vector. Figure 4 shows the

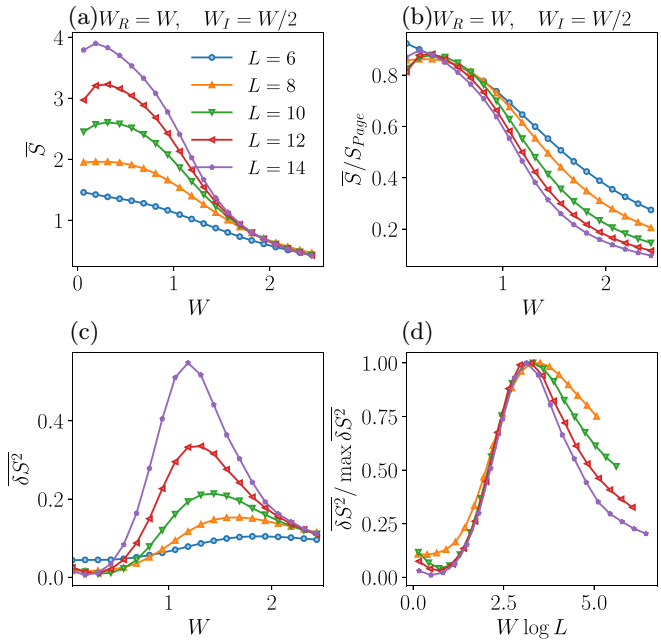

FIG. 3. MBL model: Entanglement entropy and its fluctuations in a non-Hermitian setting with $W = 2W'$. (a) $\overline{S}$ and (b) $\overline{S}/S_{\text{Page}}$ as functions of W for several system sizes L. (c) Entanglement fluctuations $\overline{\delta S^2}$ and (d) $\overline{\delta S^2}$ normalized by the maximum value. In panel (d) the disorder strength has been renormalized by multiplying by $\ln L$.

dynamics of the entanglement entropy S, as a function of time t of $|\psi(t)\rangle$, for two values of $W = 0.75, 1.25$. At $t = 0$, $S(0) = S_{\text{Page}}$, and as one can observe, the averaged entanglement entropy shows area-law scaling, $S(t)/S_{\text{Page}} \sim 1/L$; see inset in Fig. 4. This is in agreement with the numerical analysis presented in the previous section.

IV. ANALYTICAL CONSIDERATION

The aim of this section is to provide some analytical considerations that will help us to understand the enhancement of localization that we have observed numerically above.

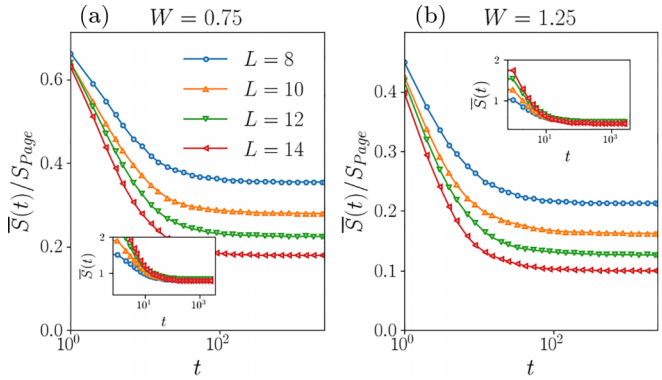

FIG. 4. MBL model: Entanglement dynamics. The entanglement dynamics of S/S_{Page} starting from a random state for (a) $W = 0.75$ and (b) $W = 1.5$. The insets show non-normalized $S(t)$ as a function of time.

A. Non-Hermitian QREM

Following the analysis presented in Ref. [99], we consider the QREM as a toy model that exhibits an MBL transition. The Hermitian QREM [100–106] is defined as

$$H_{\text{hQREM}} = \sum_{i}^{L} \sigma_i^x + W \sum_{\underline{\sigma}}^{2^L} E_{\underline{\sigma}}^R \, |\underline{\sigma}\rangle \langle \underline{\sigma}| \,, \tag{10}$$

where σ_i^x is the x Pauli matrix at site i, $\{|\underline{\sigma}\rangle\}$ are the 2^L product states, forming a basis in the σ^z Hilbert space, and $E_{\underline{\sigma}}^R$ are independent identically distributed (i.i.d.) Gaussian random variables $\mathcal{N}(0, \sqrt{L})$. From a Fock space point of view, the first term in Eq. (10) introduces jumps between z-spin configurations, which differ by one spin flip. Instead, the second term is composed of independently distributed random energies whose width scales as $\sqrt{L}$ to mimic the many-body density of states, see Eq. (13) below, given by the diagonal disorder and interaction terms. We can decompose the second term in Eq. (10) in a string composed by σ^z Pauli matrices,

$$\sum_{\underline{\sigma}}^{2^L} E_{\underline{\sigma}}^R \, |\underline{\sigma}\rangle \langle \underline{\sigma}| = \sum_{n}^{L} \sum_{i_1,\cdots,i_n} J_{i_1\cdots i_n} \sigma_{i_1}^z \cdots \sigma_{i_n}^z . \tag{11}$$

After this decomposition, we can interpret the QREM as a quantum Ising type chain subject to all possible n-body σ^z interactions, with n from 1 to L. The main difference of the QREM model from the quantum Ising model [17] is that in the latter sum, Eq. (11), only the terms with $n = 1$ and 2 survive, and coefficients $J_i, J_{i,i+1} \sim O(1)$, leading to the strong correlations between the many-body diagonal energies $E_{\underline{\sigma}}^R$.

The QREM phase diagram has been investigated in Ref. [99], finding the existence of a finite-size metal-insular transition of midspectrum states at $E = 0$, whose critical value scales as $W_c \sim \sqrt{L} \ln L$. Furthermore, H_{hQREM} has stable energy mobility edges at finite W.

In this section, we inspect the fate of the QREM under the presence of random non-Hermitian terms,

$$H_{\text{nQREM}} = \sum_{i}^{L} \sigma_i^x + W \sum_{\underline{\sigma}}^{2^L} E_{\underline{\sigma}}^R \, |\underline{\sigma}\rangle \langle \underline{\sigma}| + iW' \sum_{\underline{\sigma}}^{2^L} E_{\underline{\sigma}}^I \, |\underline{\sigma}\rangle \langle \underline{\sigma}| \,, \tag{12}$$

where $E_{\underline{\sigma}}^I$ are also i.i.d. Gaussian random variables $\mathcal{N}(0, \sqrt{L})$.

Now, we are studying the phase diagram of the non-Hermitian QREM. In the following discussion, we will demonstrate how the localization transition in the QREM, at both finite and zero energy density, is influenced by non-Hermitian gain-loss disorder.

For clarity, let us first revisit the Hermitian case.

B. Delocalization-localization transition in the Hermitian QREM analysis and comparison with the non-Hermitian case

In the Hermitian case, $E_{\underline{\sigma}}^I \equiv 0$ and real part $E_{\underline{\sigma}}^R$ is normally distributed. In particular, for the finite density energy $\epsilon = E/L$, we have for its probability

$$P\left(\frac{E_{\underline{\sigma}}^R}{L} = \epsilon\right) d\epsilon = e^{-L\epsilon^2} \sqrt{\frac{L}{\pi}} d\epsilon, \tag{13}$$

which gives the typical energy scale, given by

$$|E_0| \sim E_{\rm typ} \sim L^{1/2}. \tag{14}$$

On the localized side of the transition at large enough W, to the leading order in $1/W$ the wave-function amplitude at a certain Hilbert/Fock space node b_n at the Hamming distance n from the wave-function maximum $\psi(0)$ is

$$\psi(b_n) \simeq W^{-n} \sum_{p\in\Pi_n} \prod_{\underline{\sigma}\in p} \frac{1}{E_0 - E_{\underline{\sigma}}}, \tag{15}$$

where Π_n is the set of all $n!$ shortest directed paths between two Hilbert space nodes at the distance n, p runs over all such paths, and $\underline{\sigma}$ runs over all nodes on the path p.

The main steps to find the phase diagram of $H_{\rm hQREM}$ are the following [99]:

(i) First, we find the probability p to have a resonance at a node b_n summed over all paths at the finite-energy density, $|E_0|/L = \varepsilon > 0$, or calculated for a certain path p for the zero energy density, $\varepsilon \to 0$.

(ii) Next, we calculate the probability $P_n = (1-p)^{\mathcal{N}}$ to have no resonances in all $\mathcal{N} = \binom{L}{n}$ nodes b_n for $\varepsilon > 0$ [all $\mathcal{N} = (L)_n n!$ paths between 0 and b_n for $\varepsilon = 0$].

(iii) Then, the saddle-point approximation for $P_n \sim e^{-e^{Mf(\sigma W)}}$ is calculated over the large parameter $M = L$ ($M = n$) with the renormalized W via $\sigma = \varepsilon$ ($\sigma = \sqrt{\pi L}/2$) for $\varepsilon > 0$ ($\varepsilon = 0$).

(iv) Finally, the localization transition or the mobility edge is associated with the appearance of the first resonance when f obtains the first positive value.

Here we repeat the same argumentation for the non-Hermitian QREM model with gain-loss complex disorder potential.

First of all, in the non-Hermitian case, the eigenvalue $E_0 = E_0^R + iE_0^I \equiv L(\varepsilon^R + i\varepsilon^I)$ has both real and imaginary parts. This happens because in addition to the normal-distributed real disorder E_σ^R, there is an imaginary part, E_σ^I, which is also random and Gaussian distributed. Thus, the energy-density distribution in this case,

$$P\left(\frac{E_\sigma^R}{L} = \epsilon_R, \frac{E_\sigma^R}{L} = \epsilon_I\right) = e^{-L(\epsilon_R^2+\epsilon_I^2)}\sqrt{\frac{L}{\pi}}, \tag{16}$$

has also the Gaussian profile, but in the 2d complex plane. It is this distribution which controls the density of states, Eq. (4), of the model; therefore, similarly to the Hermitian case, the latter $\rho(E_0)$ has most of the states, concentrated at zero energy density, $\varepsilon^R = \varepsilon^I = 0$ in the thermodynamic limit. Any finite energy density (in ε^R or ε^I) will exponentially reduce the density of states with the system size. Following [99], we consider the case of the finite energy density $|E_0|/L = \varepsilon > 0$ first and then proceed to the most delocalized region of zero energy density $|E_0|/L \to 0$. Further for simplicity we consider $W = W'$, if not stated otherwise, and return back to a generic case $W \neq W'$ in the discussions later.

C. Finite energy density, $|E_0|/L = \varepsilon > 0$

In the case of finite energy density, $|E_0| \sim L$, the typical energy at the first $n-1$ nodes of the path before the resonance is of the order of $\sim L^{1/2} \ll |E_0|$ (14) and can be neglected in (15) with respect to E_0. Note that for this case the difference between QREM and the quantum Ising model, given by the correlations in (11), is not important, as the entire diagonal term can be neglected with respect to the eigenenergy E_0. Thus, the results, derived below for QREM, should be the same for the many-body problem, like the quantum Ising model.

The above approximation gives the contribution from each path to each of n neighbors a_{n-1} of b_n at the distance $n-1$ from the wave-function maximum,

$$\psi(a_{n-1}, p) \simeq \left(\frac{1}{W\varepsilon L}\right)^{-(n-1)}, \tag{17}$$

which have the same sign and, thus, can be summed coherently and the same for all a_{n-1},

$$\psi(a_{n-1}) \simeq \sum_{p\in\Pi_n} \psi(b_n, p) \simeq n!\left(\frac{1}{W\varepsilon L}\right)^{-(n-1)} \equiv \psi_{n-1}. \tag{18}$$

For resonance at b_n, one must assert that the resulting contribution to

$$\psi(b_n) \simeq \frac{n}{W\delta_n}\psi_{n-1} \tag{19}$$

should be large $|\psi(b_n)| > 1$. It can happen only if the energy difference $\delta_n = |E_0 - E_{b_n}|$ is small enough,

$$\delta_n < \delta_c \equiv \frac{n}{W}\psi_{n-1} \simeq 2L\varepsilon\sqrt{2\pi n}\left(\frac{n}{e\varepsilon WL}\right)^n. \tag{20}$$

Note that for all positive integers n the right-hand side of the latter is small compared to the width (14) of the distribution (16).

Thus, the probability p to have such a resonance is given by the following expression:

$$p = \int_{\delta_n<\delta_c} P(E_n)dE_n. \tag{21}$$

Here the main difference between Hermitian and non-Hermitian cases is in the order of the above integral over $E_n = E_n^R + iE_n^I$: it is 1d integral over i.i.d. random numbers in the Hermitian case (as $E_n^I \equiv 0$) and 2d in its non-Hermitian counterpart.

The 1d integral, corresponding to the Hermitian case of [99], immediately gives

$$p_H = P(\varepsilon)\delta_c \simeq 2\sqrt{2x}\varepsilon L \cdot e^{-L\varepsilon^2 - xL\ln[eW\varepsilon/x]}, \tag{22}$$

where $x = n/L$. Up to polynomial corrections in L, we will focus on the leading saddle-point approximation and neglect the prefactor.

The 2d integral in Eq. (21), corresponding to the non-Hermitian case, is over independent E_n^R and E_n^I, distributed according to (16). Thus, within the same approximation $\delta_n \ll \sqrt{L}$ one straightforwardly obtains

$$p_{nH} = p_H^2. \tag{23}$$

The probability P_n to not have resonances in all $\mathcal{N} = \binom{L}{n}$ directed paths connecting the stating point with b_n is given by product

$$P_n = (1-p)^{\mathcal{N}} \simeq e^{-p\mathcal{N}}, \tag{24}$$

where

$$p\mathcal{N} \simeq e^{Lf(x,p)}. \tag{25}$$

The function $f(x, p)$ differs for Hermitian and non-Hermitian cases,

$$\begin{aligned} f_H &= -x\ln x - (1-x)\ln(1-x) - \varepsilon^2 - x\ln[eW\varepsilon/x] \\ &= -(1-x)\ln(1-x) - \varepsilon^2 - x\ln[eW\varepsilon], \end{aligned} \tag{26}$$

$$\begin{aligned} f_{nH} &= -x\ln x - (1-x)\ln(1-x) - 2\varepsilon^2 - 2x\ln[eW\varepsilon/x] \\ &= x\ln x - (1-x)\ln(1-x) - \varepsilon^2 - 2x\ln[eW\varepsilon], \end{aligned} \tag{27}$$

and this provides a parametric difference between the maxima of the above functions over x at small $\varepsilon W \ll 1$,

$$x^*_H = 1 - \frac{1}{\varepsilon W}, \quad x^*_{nH} = 1 - \left(\frac{1}{\varepsilon W}\right)^2. \tag{28}$$

The latter ones, as the solutions of the equation $f(x^*, p) = 0$, lead the the parametrically different locations of the mobility edges

$$W_H^{-1} = \varepsilon + \sqrt{2}\varepsilon^2 + O(\varepsilon^3), \quad W_{nH}^{-1} = \varepsilon e^{1+\varepsilon^2}. \tag{29}$$

This is the main result for the many-body mobility edge, showing that at the same energy density, the critical disorder in the non-Hermitian case is suppressed by a factor $e^{1+\varepsilon^2}$.

The corresponding distance $n^* = x^*L$, where the first resonance to appear is also parametrically different,

$$x^*_H = \sqrt{2}\varepsilon + O(\varepsilon^2), \quad x^*_{nH} = 1 - e^{-2(1+\varepsilon^2)}. \tag{30}$$

Here, the main difference between the Hermitian and non-Hermitian cases is that the first resonance at zero energy density in the former case appears at very short distances, where $n^*/L \to 0$, and approaches zero, while in the latter case, it remains finite, resulting in sharper mobility edges.

D. Zero energy density, $|E_0|/L = \varepsilon = 0$

Unlike the previous case, here the terms of the different paths to b_n are not coherent due to the random signs (or even complex phases) of the denominators in Eq. (15) and this forces us to consider all $\frac{\mathcal{N}=(L}{n)n!}$ paths independently and assume that the first resonance appears only on one of them [107].

Following [99], we introduce a random variable

$$y_{\underline{\sigma}} = \ln(\sigma/|E_{\underline{\sigma}}|) \quad \Leftrightarrow \quad |E_{\underline{\sigma}}| = \sigma e^{-y_{\underline{\sigma}}}, \tag{31}$$

where $\sigma = \sqrt{\pi L}/2$ is chosen in such a way to make the distribution $P(y_{\underline{\sigma}} \gtrsim 1)$ to be parameter free. Here again the main difference between Hermitian and non-Hermitian cases appears, due to the dimensionality of the distributions (13) and (16). Indeed, for the Hermitian case one obtains

$$P(y_{\underline{\sigma}} = y) = P(\epsilon)\frac{d\epsilon}{dy} = e^{-y-\frac{\pi}{4}e^{-2y}} \quad \Leftrightarrow \quad P(y \gtrsim 1) \simeq e^{-y}, \tag{32}$$

while in the non-Hermitian case, the results are more involved,

$$\begin{aligned} P(y) &= \int \frac{e^{-(E_R^2+E_I^2)/L}}{\pi L}\delta\left(y + \frac{1}{2}\ln\left[\frac{E_R^2+E_I^2}{\sigma^2}\right]\right)dE_R dE_I \\ &= \frac{e^{-\frac{\pi}{4}e^{-2y}}}{\pi L}\int_{-\sigma e^{-y}}^{\sigma e^{-y}} \frac{\partial E_R(y, E_I)}{\partial y} dE_I \\ &= \frac{2e^{-\frac{\pi}{4}e^{-2y}}}{\pi L}\sigma^2 e^{-2y}\int_{-1}^{1}\frac{dz}{\sqrt{1-z^2}} \\ &= \pi e^{-\frac{\pi}{4}e^{-2y}-2y}, \end{aligned} \tag{33}$$

where we used the expression $E_R(y, E_I) = \sqrt{\sigma^2 e^{-2y} - E_I^2}$ and $z = E_I e^y/\sigma$.

The first resonance appears at b_n as soon as

$$\ln|\psi(b_n)| > 1 \quad \Leftrightarrow \quad Y_n = \sum_{\underline{\sigma}=1}^{n} y_{\underline{\sigma}} > Y_c, \tag{34}$$

where we have introduced the critical value as $Y_c \equiv n\ln(\sigma W)$ and numbered the nodes $\underline{\sigma}$ via the distance from the wavefunction maximum.

In our approximation of $|y_{\underline{\sigma}}| \gtrsim 1$, the distribution of $P(Y)$ reads slightly differently for Hermitian,

$$P_H(Y) \simeq \frac{Y^{n-1}}{(n-1)!}e^{-Y} \simeq \left(\frac{Ye}{n}\right)^n e^{-Y}, \tag{35}$$

and non-Hermitian cases,

$$P_{nH}(Y) \simeq \frac{(2Y)^{n-1}}{2(n-1)!}e^{-2Y} \simeq \left(\frac{2Ye}{n}\right)^n e^{-2Y}. \tag{36}$$

However, these are factors of 2 which parametrically change the critical disorder amplitude, as they appear in front of the logarithmic factors in $Y_c \equiv n\ln(\sigma W)$.

For large enough $Y_c = n\ln(\sigma W) \gg 1$ the probability to have a resonance (34) is given by

$$p = P(Y_c)\left[1 + O\left(Y_c^{-1}\right)\right]; \tag{37}$$

thus, the probability to have no resonances for all $\frac{\mathcal{N}=(L}{n)n!\simeq L^n}$ paths reads exactly as (24), leading to the following saddle-point approximation over n,

$$p\mathcal{N} = e^{nf(\sigma W)}, \tag{38}$$

with f being different for the two above cases via the constant c,

$$\begin{aligned} f(\sigma W) &\equiv \ln L + \frac{1}{n}\ln[P(Y_c)] \\ &= \ln(eL) - c\ln(\sigma W) + \ln[c\ln(\sigma W)]. \end{aligned} \tag{39}$$

$c = 1$ for Hermitian and $c = 2$ for non-Hermitian cases.

Again, such a tiny difference in the prefactors in front of the logarithms leads to the parametric difference in critical disorder values between these cases as the leading in L solution is

$$(\sigma W)^c \simeq eL\ln(eL) \quad \Leftrightarrow \quad W = \frac{2}{\sqrt{\pi}}L^{1/c-1/2}[e\ln(eL)]^{1/c}. \tag{40}$$

Here, the Hermitian case of $c = 1$ gives the standard result

$$W_H \sim L^{1/2} \ln L, \tag{41}$$

while the 2d nature, $c = 2$, of the diagonal disorder in the gain-loss non-Hermitian case leads to the completely unexpected one:

$$W_{nH} \sim \ln^{1/2} L. \tag{42}$$

This comparison shows the drastic difference between Hermitian and non-Hermitian cases as in the limit of large L, $W_{nH} \ll W_H$, and their ratio goes to zero.

The origin of this drastic change lies in the resonance counting difference (see also [82]). Indeed, the probability of a resonance to occur at the distance n is directly related to the mean level spacing Δ_n between the on-site energies $E_{\underline{\sigma}}$ on all the K_n nodes $\underline{\sigma}$, close to the maximum $|\underline{\sigma}| < n$ (K_n is the number of such nodes). However, it is Δ_n which is parametrically different in Hermitian and non-Hermitian cases.

In the Hermitian case the mean level spacing is given by $\Delta_n^H \simeq WL^{1/2}/K_n$ as in the typical 1d interval $|E_{\underline{\sigma}}| \lesssim WL^{1/2}$ there are K_n i.i.d. random numbers. At the same time, gain-loss non-Hermiticity allows $E_{\underline{\sigma}} = E_{\underline{\sigma}}^R + iE_{\underline{\sigma}}^I$ to be distributed in the 2d complex plane in the typical range $|E_{\underline{\sigma}}^R| < WL^{1/2}$, $|E_{\underline{\sigma}}^I| < W'L^{1/2}$, leading to the mean area per on-site energy, given by $A_n \simeq WW'L/K_n$. The mean radius of such area estimates the mean level spacing as $\Delta_n^{nH} \sim A_n^{1/2} \simeq (WW'L/K_n)^{1/2}$ which decays with K_n parametrically slower than Δ_n^H. For more detailed discussion please see [82]. Here we have returned back to the generic case of $W \neq W'$ to show that the main claim is intact with respect to the ratio W/W' as soon as the latter is finite.

The latter consideration as well as the entire derivation in Sec. IV C are consistent with the generic consideration of the Hermitian case, where the ratio W_0/t of the standard deviation of the diagonal $\langle |E_{\underline{\sigma}}|^2 \rangle^{1/2} = W_0$ and the hopping t terms at the critical point is given by the function of the vertex degree $d \gg 1$ of the corresponding graph

$$\left(\frac{W_0}{t}\right) = d \ln d. \tag{43}$$

Without $\ln d$ this is related to the number of possibilities to realize the resonance with any of d neighbors at $n = 1$ at large W_0; therefore the probability to have a resonance energy is given by the inverse of the latter, i.e., by the first power t/W_0. The factor $\ln d$ appears due to the hierarchical structure of the underlying graph; see, e.g., [99].

In the non-Hermitian case with the same variances for real and imaginary parts, $\langle E_{n,R}^2 \rangle^{1/2} = \langle E_{n,I}^2 \rangle^{1/2} = W_0$, the above probability of having small $|E_n - E_0|$ is given by $(t/W_0)^2$ as each of real and imaginary parts should be in the vicinity t from $E_{0,R/I}$, respectively. Thus, in this case one should expect

$$\left(\frac{W_0}{t}\right)^2 = d \ln d. \tag{44}$$

The case of $W \neq W'$ will correspond here to the additional prefactor on the left-hand side given by W'/W, but will not change qualitatively the result.

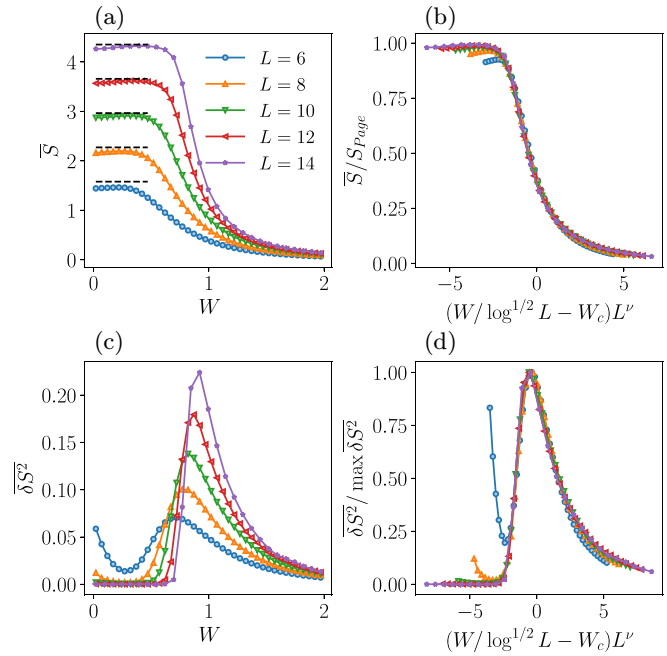

FIG. 5. QREM model: Entanglement entropy and its fluctuations in a non-Hermitian setting of Eq. (12). (a) $\overline{S}$, as a function of W for several L; (b) finite-size collapse of $\overline{S}/S_{\text{Page}}$. The panel shows that the critical value shifts to larger values as $\ln^{1/2}(L)$. (c) Fluctuations $\overline{\delta S^2}$ of S and (d) finite-size collapse of $\overline{\delta S^2}$, normalized by its maximal value. In both panels (b) and (d) the finite-size collapse gives $W_c \approx 0.5$ and $\nu \approx 1$.

The above estimates (43) and (44) are consistent with both the above results (41) and (42), where $d = L$, $t = 1$, and $W_0 = \sigma W = \sqrt{\pi L} W/2$. At the same time, Eqs. (43) and (44) give the correct result for the Rosenzweig-Porter model [81], where $d = N$, $t = N^{-\gamma/2}$, $W_0 = 1$.

E. Numerical result for the non-Hermitian QREM

After providing an analytical perspective on the non-Hermitian QREM, which reveals that the model is substantially more localized compared to its Hermitian counterpart, we proceed to the numerical validation of our hypotheses. The probes employed for this validation are the same as those utilized for the random-field Heisenberg model, Eq. (2), that serve to distinguish extended and localized phases.

Figures 5 and 6 focus on the entanglement entropy and fractal dimension, respectively, and their associated fluctuations. Within both figures, panels (a) and (c) display the raw data as a function of W across various system sizes. As expected, the range in which the model exhibits delocalization, denoted $S/S_{\text{Page}} \to 1$ and $D_2 \to 1$, broadens with the system size L. Fingerprints of the transition are given to the moving maximum of the fluctuations of S and D_2 visible in Figs. 5(c) and 6(c), respectively. To find the scaling of the value of the critical point with system size, we perform a finite-size scaling analysis, which is shown in Figs. 5(b), 5(d) and Figs. 6(b), 6(d). As expected from our analytical considerations, we found with $W_c \sim \ln^{1/2} L$ a good collapse of the curves.

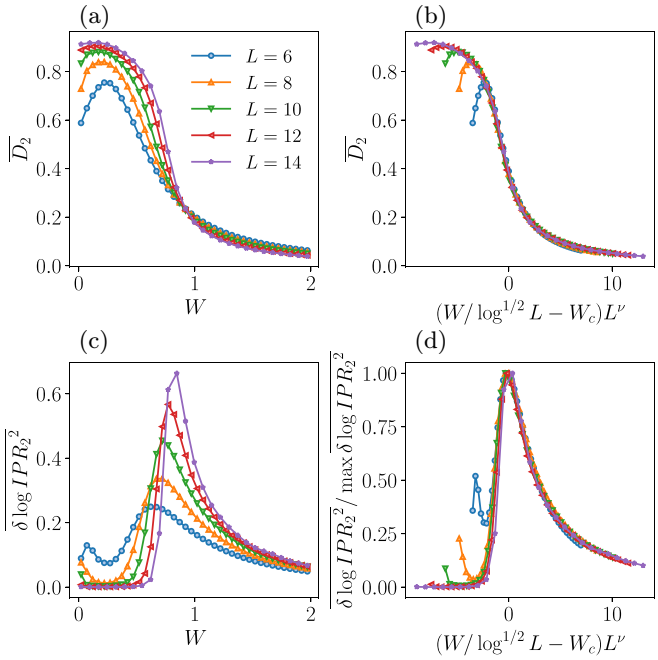

FIG. 6. QREM model: Fractal dimension D_2 and its fluctuations in a non-Hermitian setting of Eq. (12). (a) $\overline{D}_2$ as a function of W for several L; (c) fluctuations $\overline{\delta \ln IPR_2{}^2}$ of $-\ln IPR_2$. (b), (d) Finite-size collapses of $\overline{D}_2$ and $\overline{\delta \ln IPR_2{}^2}$, normalized by its maximal value, giving the same critical values $W_c = 0.5$ and $\nu \approx 1$ as in Fig. 5.

V. OUTLOOK AND CONCLUSION

In this work, we examine the phase of the random-field Heisenberg model under monitoring in the no-click limit. Without monitoring, the model is believed to exhibit a many-body localization transition, which separates an ergodic phase at weak disorder from a localized one at strong disorder.

Under random-space continuous monitoring in the no-click limit, the model is mapped to a non-Hermitian system with complex random diagonal disorder. Numerically, we investigate the localization properties of the model, in particular, the entanglement entropy and the fractal dimension in the Fock space. We found that the model exhibits a more robust form of localization. We provide a finite-size scale analysis, which suggests that the extended phase disappears in the thermodynamic limit, leaving the system in MBL for any finite amount of disorder. It is important to note that in the case of continuous but nonrandom measurements in space, the model is expected to exhibit the typical MBL transition, as demonstrated in Ref. [46].

Although we do not have an analytical approach for our random-field Heidelberg model, we consider the non-Hermitian analog of the QREM as a toy and analytically tractable model to test our conjectures. In the past, the Hermitian QREM has been used to describe the MBL transition, providing evidence of MBL and the existence of many-body mobility edges. We consider a non-Hermitian version of the QREM, which mimics our random gain and loss terms. Using a self-consistent theory of localization, we show that the non-Hermitian QREM exhibits sharp many-body mobility edges, and the system is parametrically more localized than its corresponding Hermitian counterpart. From the many-body point of view, the QREM in Eq. (12) has more long-range interaction terms, and therefore the Anderson transition as well as the mobility edge in the non-Hermitian QREM should provide upper bounds for the MBL transition and the many-body mobility edge (at least for the quantum Ising model). From Eqs. (29) and (42) and their comparison to the numerical calculations in Figs. 1 and 2, one sees that this upper bound is not strict.

Our work establishes the foundation for stabilizing phases of matter through the application of random gain and loss terms. Future studies will investigate the potential of this measurement protocol to stabilize many-body localized topological phases and to induce localization in systems with higher dimensions and long-range interactions. Additionally, promising avenues of research include examining the effects of non-Hermitian elements on the avalanche theory of delocalization, as well as their influence on real-time dynamics [50,51].

ACKNOWLEDGMENTS

We are grateful to J. Bardarson, D. Belkin, B. Clark, R. Hamazaki, M. Ippoliti, M. Schiro, K. Su, F. Roccati, and S. Vijay for stimulating discussion. We also express our gratitude to R. Hamazaki and M. Schiro for comments and a critical reading of the manuscript. I.M.K. acknowledges support by the European Research Council under the European Union's Seventh Framework Program Synergy ERC-2018-SyG HERO-810451. G.D.T. acknowledges support from the EPiQS Program of the Gordon and Betty Moore Foundation.

[1] J. M. Deutsch, Quantum statistical mechanics in a closed system, Phys. Rev. A **43**, 2046 (1991).

[2] Rigol Marcos, D. Vanja, and O. Maxim, Thermalization and its mechanism for generic isolated quantum systems, Nature (London) **452**, 854 (2008).

[3] L. D'Alessio, Y. Kafri, A. Polkovnikov, and M. Rigol, From quantum chaos and eigenstate thermalization to statistical mechanics and thermodynamics, Adv. Phys. **65**, 239 (2016).

[4] D. M. Basko, I. L. Aleiner, and B. L. Altshuler, Metal-insulator transition in a weakly interacting many-electron system with localized single-particle states, Ann. Phys. **321**, 1126 (2006).

[5] I. V. Gornyi, A. D. Mirlin, and D. G. Polyakov, Interacting electrons in disordered wires: Anderson localization and low-T transport, Phys. Rev. Lett. **95**, 206603 (2005).

[6] R. Nandkishore and D. A. Huse, Many-body localization and thermalization in quantum statistical mechanics, Annu. Rev. Condens. Matter Phys. **6**, 15 (2015).

[7] D. A. Abanin, E. Altman, I. Bloch, and M. Serbyn, *Colloquium:* Many-body localization, thermalization, and entanglement, Rev. Mod. Phys. **91**, 021001 (2019).

[8] E. Canovi, D. Rossini, R. Fazio, G. E. Santoro, and A. Silva, Quantum quenches, thermalization, and many-body localization, Phys. Rev. B **83**, 094431 (2011).

[9] J. Richter and A. Pal, Many-body localization and delocalization dynamics in the thermodynamic limit, Phys. Rev. B **105**, L220405 (2022).

[10] M. Serbyn, Z. Papić, and D. A. Abanin, Thouless energy and multifractality across the many-body localization transition, Phys. Rev. B **96**, 104201 (2017).

[11] S. Gopalakrishnan and S. A. Parameswaran, Dynamics and transport at the threshold of many-body localization, Phys. Rep. **862**, 1 (2020).

[12] F. Kotthoff, F. Pollmann, and G. De Tomasi, Distinguishing an Anderson insulator from a many-body localized phase through space-time snapshots with neural networks, Phys. Rev. B **104**, 224307 (2021).

[13] E. J. Torres-Herrera, G. De Tomasi, M. Schiulaz, F. Pérez-Bernal, and L. F. Santos, Self-averaging in many-body quantum systems out of equilibrium: Approach to the localized phase, Phys. Rev. B **102**, 094310 (2020).

[14] J. H. Bardarson, F. Pollmann, and J. E. Moore, Unbounded growth of entanglement in models of many-body localization, Phys. Rev. Lett. **109**, 017202 (2012).

[15] M. Serbyn, Z. Papić, and D. A. Abanin, Local conservation laws and the structure of the many-body localized states, Phys. Rev. Lett. **111**, 127201 (2013).

[16] M. Serbyn, Z. Papić, and D. A. Abanin, Quantum quenches in the many-body localized phase, Phys. Rev. B **90**, 174302 (2014).

[17] J. Z. Imbrie, On many-body localization for quantum spin chains, J. Stat. Phys. **163**, 998 (2016).

[18] D. A. Huse, R. Nandkishore, and V. Oganesyan, Phenomenology of fully many-body-localized systems, Phys. Rev. B **90**, 174202 (2014).

[19] V. Ros, M. Müller, and A. Scardicchio, Integrals of motion in the many-body localized phase, Nucl. Phys. B **891**, 420 (2015).

[20] M. Serbyn, Z. Papić, and D. A. Abanin, Universal slow growth of entanglement in interacting strongly disordered systems, Phys. Rev. Lett. **110**, 260601 (2013).

[21] G. De Tomasi, F. Pollmann, and M. Heyl, Efficiently solving the dynamics of many-body localized systems at strong disorder, Phys. Rev. B **99**, 241114(R) (2019).

[22] M. Serbyn, D. A. Abanin, and Z. Papić, Quantum many-body scars and weak breaking of ergodicity, Nat. Phys. **17**, 675 (2021).

[23] S. Moudgalya, N. Regnault, and B. A. Bernevig, Entanglement of exact excited states of Affleck-Kennedy-Lieb-Tasaki models: Exact results, many-body scars, and violation of the strong eigenstate thermalization hypothesis, Phys. Rev. B **98**, 235156 (2018).

[24] G. De Tomasi, D. Hetterich, P. Sala, and F. Pollmann, Dynamics of strongly interacting systems: From Fock-Space fragmentation to many-body localization, Phys. Rev. B **100**, 214313 (2019).

[25] S. Moudgalya, B. A. Bernevig, and N. Regnault, Quantum many-body scars and Hilbert space fragmentation: a review of exact results, Rep. Prog. Phys. **85**, 086501 (2022).

[26] S. Moudgalya and O. I. Motrunich, Hilbert space fragmentation and commutant algebras, Phys. Rev. X **12**, 011050 (2022).

[27] A. Smith, J. Knolle, D. L. Kovrizhin, and R. Moessner, Disorder-free localization, Phys. Rev. Lett. **118**, 266601 (2017).

[28] M. Brenes, M. Dalmonte, M. Heyl, and A. Scardicchio, Many-body localization dynamics from gauge invariance, Phys. Rev. Lett. **120**, 030601 (2018).

[29] A. Russomanno, S. Notarnicola, F. M. Surace, R. Fazio, M. Dalmonte, and M. Heyl, Homogeneous Floquet time crystal protected by gauge invariance, Phys. Rev. Res. **2**, 012003(R) (2020).

[30] P. Karpov, R. Verdel, Y.-P. Huang, M. Schmitt, and M. Heyl, Disorder-free localization in an interacting 2D lattice gauge theory, Phys. Rev. Lett. **126**, 130401 (2021).

[31] X. Chen, Y. Li, M. P. A. Fisher, and A. Lucas, Emergent conformal symmetry in nonunitary random dynamics of free fermions, Phys. Rev. Res. **2**, 033017 (2020).

[32] Q. Tang, X. Chen, and W. Zhu, Quantum criticality in the nonunitary dynamics of $(2+1)$-dimensional free fermions, Phys. Rev. B **103**, 174303 (2021).

[33] Y. Li, X. Chen, and M. P. A. Fisher, Quantum Zeno effect and the many-body entanglement transition, Phys. Rev. B **98**, 205136 (2018).

[34] Y. Li, X. Chen, and M. P. A. Fisher, Measurement-driven entanglement transition in hybrid quantum circuits, Phys. Rev. B **100**, 134306 (2019).

[35] B. Skinner, J. Ruhman, and A. Nahum, Measurement-induced phase transitions in the dynamics of entanglement, Phys. Rev. X **9**, 031009 (2019).

[36] A. Zabalo, M. J. Gullans, J. H. Wilson, R. Vasseur, A. W. W. Ludwig, S. Gopalakrishnan, D. A. Huse, and J. H. Pixley, Operator scaling dimensions and multifractality at measurement-induced transitions, Phys. Rev. Lett. **128**, 050602 (2022).

[37] A. Chan, R. M. Nandkishore, M. Pretko, and G. Smith, Unitary-projective entanglement dynamics, Phys. Rev. B **99**, 224307 (2019).

[38] K. Jacobs and D. A. Steck, A straightforward introduction to continuous quantum measurement, Contemp. Phys. **47**, 279 (2006).

[39] A. Paviglianiti, X. Turkeshi, M. Schirò, and A. Silva, Enhanced entanglement in the measurement-altered quantum Ising chain, arXiv:2310.02686.

[40] G. Passarelli, X. Turkeshi, A. Russomanno, P. Lucignano, M. Schirò, and R. Fazio, Many-body dynamics in monitored atomic gases without postselection barrier, Phys. Rev. Lett. **132**, 163401 (2024).

[41] Y. L. Gal, X. Turkeshi, and M. Schirò, Volume-to-area law entanglement transition in a non-Hermitian free fermionic chain, SciPost Phys. **14**, 138 (2023).

[42] X. Cao, A. Tilloy, and A. D. Luca, Entanglement in a fermion chain under continuous monitoring, SciPost Phys. **7**, 024 (2019).

[43] H. M. Wiseman and G. J. Milburn, *Quantum Measurement and Control* (Cambridge University Press, Cambridge, 2009).

[44] Y. Ashida, Z. Gong, and M. Ueda, Non-Hermitian physics, Adv. Phys. **69**, 249 (2020).

[45] S. Gopalakrishnan and M. J. Gullans, Entanglement and purification transitions in non-Hermitian quantum mechanics, Phys. Rev. Lett. **126**, 170503 (2021).

[46] K. Yamamoto and R. Hamazaki, Localization properties in disordered quantum many-body dynamics under continuous measurement, Phys. Rev. B **107**, L220201 (2023).

[47] Q. Liu, K. Ziegler, D. A. Kessler, and E. Barkai, Driving quantum systems with periodic conditional measurements, Phys. Rev. Res. **4**, 023129 (2022).

[48] X.-J. Yu, Z. Pan, L. Xu, and Z.-X. Li, Non-Hermitian strongly interacting Dirac fermions, Phys. Rev. Lett. **132**, 116503 (2024).

[49] Z.-X. Guo, X.-J. Yu, X.-D. Hu, and Z. Li, Emergent phase transitions in a cluster Ising model with dissipation, Phys. Rev. A **105**, 053311 (2022).

[50] X. Turkeshi, A. Biella, R. Fazio, M. Dalmonte, and M. Schiró, Measurement-induced entanglement transitions in the quantum Ising chain: From infinite to zero clicks, Phys. Rev. B **103**, 224210 (2021).

[51] X. Turkeshi and M. Schiró, Entanglement and correlation spreading in non-Hermitian spin chains, Phys. Rev. B **107**, L020403 (2023).

[52] C. Zerba and A. Silva, Measurement phase transitions in the no-click limit as quantum phase transitions of a non-Hermitean vacuum, SciPost Phys. Core **6**, 051 (2024).

[53] S.-Z. Li, X.-J. Yu, and Z. Li, Emergent entanglement phase transitions in non-Hermitian Aubry-André-Harper chains, Phys. Rev. B **109**, 024306 (2024).

[54] E. J. Bergholtz, J. C. Budich, and F. K. Kunst, Exceptional topology of non-Hermitian systems, Rev. Mod. Phys. **93**, 015005 (2021).

[55] R. Lin, T. Tai, L. Li, and C. H. Lee, Topological non-Hermitian skin effect, Front. Phys. **18**, 53605 (2023).

[56] X. Zhang, T. Zhang, M.-H. Lu, and Y.-F. Chen, A review on non-Hermitian skin effect, Adv. Phys.: X **7**, 2109431 (2022).

[57] N. Okuma and M. Sato, Non-Hermitian topological phenomena: A review, Annu. Rev. Condens. Matter Phys. **14**, 83 (2023).

[58] K. Kawabata, T. Numasawa, and S. Ryu, Entanglement phase transition induced by the non-Hermitian skin effect, Phys. Rev. X **13**, 021007 (2023).

[59] N. Hatano and D. R. Nelson, Localization transitions in non-Hermitian quantum mechanics, Phys. Rev. Lett. **77**, 570 (1996).

[60] R. Hamazaki, K. Kawabata, and M. Ueda, Non-Hermitian many-body localization, Phys. Rev. Lett. **123**, 090603 (2019).

[61] L.-J. Zhai, S. Yin, and G.-Y. Huang, Many-body localization in a non-Hermitian quasiperiodic system, Phys. Rev. B **102**, 064206 (2020).

[62] K. Suthar, Y.-C. Wang, Y.-P. Huang, H. H. Jen, and J.-S. You, Non-Hermitian many-body localization with open boundaries, Phys. Rev. B **106**, 064208 (2022).

[63] Y.-C. Wang, K. Suthar, H. H. Jen, Y.-T. Hsu, and J.-S. You, Non-Hermitian skin effects on thermal and many-body localized phases, Phys. Rev. B **107**, L220205 (2023).

[64] H.-Z. Li, X.-J. Yu, and J.-X. Zhong, Non-Hermitian stark many-body localization, Phys. Rev. A **108**, 043301 (2023).

[65] J. Mák, M. J. Bhaseen, and A. Pal, Statics and dynamics of non-Hermitian many-body localization, Commun. Phys. **7**, 92 (2024).

[66] A. Pal and D. A. Huse, Many-body localization phase transition, Phys. Rev. B **82**, 174411 (2010).

[67] D. J. Luitz, N. Laflorencie, and F. Alet, Many-body localization edge in the random-field Heisenberg chain, Phys. Rev. B **91**, 081103(R) (2015).

[68] S. Bera, H. Schomerus, F. Heidrich-Meisner, and J. H. Bardarson, Many-body localization characterized from a one-particle perspective, Phys. Rev. Lett. **115**, 046603 (2015).

[69] T. Devakul and R. R. P. Singh, Early breakdown of area-law entanglement at the many-body delocalization transition, Phys. Rev. Lett. **115**, 187201 (2015).

[70] P. Sierant, M. Lewenstein, and J. Zakrzewski, Polynomially filtered exact diagonalization approach to many-body localization, Phys. Rev. Lett. **125**, 156601 (2020).

[71] S. Vardhan, G. De Tomasi, M. Heyl, E. J. Heller, and F. Pollmann, Characterizing time irreversibility in disordered fermionic systems by the effect of local perturbations, Phys. Rev. Lett. **119**, 016802 (2017).

[72] S. Bera, G. De Tomasi, F. Weiner, and F. Evers, Density propagator for many-body localization: Finite-size effects, transient subdiffusion, and exponential decay, Phys. Rev. Lett. **118**, 196801 (2017).

[73] G. De Tomasi, S. Bera, J. H. Bardarson, and F. Pollmann, Quantum mutual information as a probe for many-body localization, Phys. Rev. Lett. **118**, 016804 (2017).

[74] E. V. H. Doggen, F. Schindler, K. S. Tikhonov, A. D. Mirlin, T. Neupert, D. G. Polyakov, and I. V. Gornyi, Many-body localization and delocalization in large quantum chains, Phys. Rev. B **98**, 174202 (2018).

[75] N. Mott and W. Twose, The theory of impurity conduction, Adv. Phys. **10**, 107 (1961).

[76] P. W. Anderson, Absence of diffusion in certain random lattices, Phys. Rev. **109**, 1492 (1958).

[77] In the standard setting γ_x are considered to be non-negative, thus, having only losses. We consider the case of gains and losses, balanced on average, though it can be considered as a shift of the overall energy by W.

[78] J. P. Pekola, B. Karimi, M. Cattaneo, and S. Maniscalco, Long-time relaxation of a finite spin bath linearly coupled to a qubit, Open Syst. Inf. Dyn. **30**, 2350009 (2023).

[79] Y. Huang and B. I. Shklovskii, Anderson transition in three-dimensional systems with non-Hermitian disorder, Phys. Rev. B **101**, 014204 (2020).

[80] Y. Huang and B. I. Shklovskii, Spectral rigidity of non-Hermitian symmetric random matrices near the Anderson transition, Phys. Rev. B **102**, 064212 (2020).

[81] G. De Tomasi and I. M. Khaymovich, Non-Hermitian Rosenzweig-Porter random-matrix ensemble: Obstruction to the fractal phase, Phys. Rev. B **106**, 094204 (2022).

[82] G. De Tomasi and I. M. Khaymovich, Non-Hermiticity induces localization: Good and bad resonances in power-law random banded matrices, Phys. Rev. B **108**, L180202 (2023).

[83] We focus on the right eigenvectors, as we do not observe any significant difference with the left eigenvector, belonging to the middle of the spectrum.

[84] D. N. Page, Average entropy of a subsystem, Phys. Rev. Lett. **71**, 1291 (1993).

[85] Y. Huang, Universal eigenstate entanglement of chaotic local Hamiltonians, Nucl. Phys. B **938**, 594 (2019).

[86] M. Haque, P. A. McClarty, and I. M. Khaymovich, Entanglement of midspectrum eigenstates of chaotic many-body systems: Reasons for deviation from random ensembles, Phys. Rev. E **105**, 014109 (2022).

[87] Y. Huang, Universal entanglement of mid-spectrum eigenstates of chaotic local Hamiltonians, Nucl. Phys. B **966**, 115373 (2021).

[88] M. Kliczkowski, R. Świetek, L. Vidmar, and M. Rigol, Average entanglement entropy of midspectrum eigenstates of quantum-chaotic interacting Hamiltonians, Phys. Rev. E **107**, 064119 (2023).

[89] A. Sarkar and S. Kumar, Entanglement spectrum statistics of a time reversal invariant spin chain system: insights from random matrix theory, Eur. Phys. J. B **96**, 120 (2023).

[90] N. Macé, F. Alet, and N. Laflorencie, Multifractal scalings across the many-body localization transition, Phys. Rev. Lett. **123**, 180601 (2019).

[91] A. D. Luca and A. Scardicchio, Ergodicity breaking in a model showing many-body localization, Europhys. Lett. **101**, 37003 (2013).

[92] K. S. Tikhonov and A. D. Mirlin, Many-body localization transition with power-law interactions: Statistics of eigenstates, Phys. Rev. B **97**, 214205 (2018).

[93] D. A. Abanin, J. Bardarson, G. De Tomasi, S. Gopalakrishnan, V. Khemani, S. A. Parameswaran, F. Pollmann, A. C. Potter, M. Serbyn, and R. Vasseur, Distinguishing localization from chaos: Challenges in finite-size systems, Ann. Phys. **427**, 168415 (2021).

[94] J. Šuntajs, J. Bonča, T. Prosen, and L. Vidmar, Quantum chaos challenges many-body localization, Phys. Rev. E **102**, 062144 (2020).

[95] D. Sels and A. Polkovnikov, Dynamical obstruction to localization in a disordered spin chain, Phys. Rev. E **104**, 054105 (2021).

[96] J. Sirker, Exploration of the existence of a distinct quasi many-body localized phase: Numerical study of a translationally invariant system in the thermodynamic limit, Phys. Rev. B **99**, 075162 (2019).

[97] G. De Tomasi, I. M. Khaymovich, F. Pollmann, and S. Warzel, Rare thermal bubbles at the many-body localization transition from the Fock space point of view, Phys. Rev. B **104**, 024202 (2021).

[98] Note that in the case of nonreciprocal hopping, the peak of the entanglement fluctuations does not develop; see, e.g., [60].

[99] C. R. Laumann, A. Pal, and A. Scardicchio, Many-body mobility edge in a mean-field quantum spin glass, Phys. Rev. Lett. **113**, 200405 (2014).

[100] C. L. Baldwin, C. R. Laumann, A. Pal, and A. Scardicchio, The many-body localized phase of the quantum random energy model, Phys. Rev. B **93**, 024202 (2016).

[101] G. Biroli, D. Facoetti, M. Schiró, M. Tarzia, and P. Vivo, Out-of-equilibrium phase diagram of the quantum random energy model, Phys. Rev. B **103**, 014204 (2021).

[102] L. Faoro, M. V. Feigel'man, and L. Ioffe, Non-ergodic extended phase of the quantum random energy model, Ann. Phys. **409**, 167916 (2019).

[103] T. Parolini and G. Mossi, Multifractal dynamics of the QREM, arXiv:2007.00315.

[104] V. N. Smelyanskiy, K. Kechedzhi, S. Boixo, S. V. Isakov, H. Neven, and B. Altshuler, Nonergodic delocalized states for efficient population transfer within a narrow band of the energy landscape, Phys. Rev. X **10**, 011017 (2020).

[105] K. Kechedzhi, V. N. Smelyanskiy, J. R. McClean, V. S. Denchev, M. Mohseni, S. V. Isakov, S. Boixo, B. L. Altshuler, and H. Neven, Efficient population transfer via non-ergodic extended states in quantum spin glass, arXiv:1807.04792.

[106] V. N. Smelyanskiy, K. Kechedzhi, S. Boixo, H. Neven, and B. Altshuler, Intermittency of dynamical phases in a quantum spin glass, arXiv:1907.01609.

[107] Note that it is not the case for the MBL problems, where the resonances appear simultaneously due to the strong correlations in the diagonal energy, Eq. (11).